Design, Manufacture, Modeling and Testing of 316 SS Diffusion Bonded Tube-sheet Joints and In-Service Inspection Methods for the Mk1 PB-FHR CTAHs

NE 170 – Senior Design Project

Grant Buster, Nathan Pardede, and Tung Phan
Department of Nuclear Engineering
University of California, Berkeley

Report UCBTH-14-005

Final_Report

15 May, 2014

ABSTRACT

This report presents the primary findings on design, fabrication, and performance characteristics of diffusion-bonded 316 SS tube to tube-sheet joints that are used in the Mk1 PB-FHR Coiled Tube Air Heaters (CTAHs), as well as findings on the feasibility of in-service inspection for coiled tubes. Two prototype CTAHs joints were machined out of the 316 stainless steel. Both sample joints underwent high compressive forces at 1000 ºC in different furnaces for 1000 minutes using methods recommended by Clark and Mizia at Idaho National Laboratory, producing diffusion bonds of varying strengths. This successfully demonstrates diffusion bonding as a viable manufacturing technique that will deliver a strong joint. Optical examination of axial and circumferential cross-sections of the diffusion bonded samples will be useful in characterizing the bond, in order to increase the level of confidence in the bond strength. Additional investigation included Finite Element Modeling (FEM) analysis to study stresses in diffusion bonded joints under service conditions. Likewise, a method for performing eddy-current in-service inspection of CTAH tubes was studied using a mockup for a small-scale tube inspection probe. Future work should examine experimentally the use of stress relief groves around the outside of the tube-sheet hole to reduce the stress concentration in this area, which should aid to prevent delamination and further strengthen the joints.

TABLE OF CONTENTS

TABLE OF FIGURES

1.0 INTRODUCTION

In the Mk1 Pebble Bed Fluoride Salt Cooled High Temperature Reactor (Mk1 PB-FHR) (Andreades et al., 2014), Coiled Tube Air Heaters (CTAHs) are used to transfer heat between the primary loop (fluoride salt) and the power conversion fluid (compressed air). The baseline material for the Mk1 CTAHs is 316 stainless steel (316 SS), although other materials such as 304 SS and Alloy N are also candidates for use in FHRs. Figure 1 shows an isometric view of a CTAHs sub-bundle, showing how salt flows from outside manifold pipes through the coiled bundle to the inside manifold pipes. Multiple sub-bundles form the full heat exchanger. Fabrication of these CTAHs requires the bonding of tubes to tube-sheets. Figure 2 shows a detailed view of where diffusion bonds are necessary. This project studied the possibility of fabricating these bonds using diffusion bonding methods, as well as the possibility of modeling these bonds using finite element modeling (FEM).

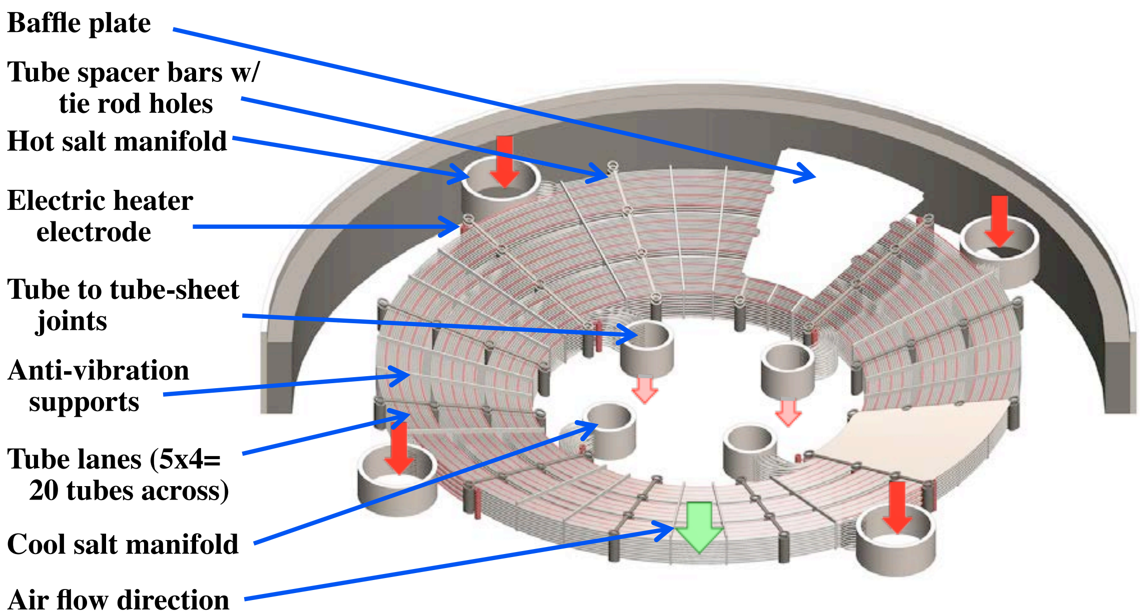

Figure 1. Each Mk1 CTAHs has 36 sub-bundles, as pictured here.

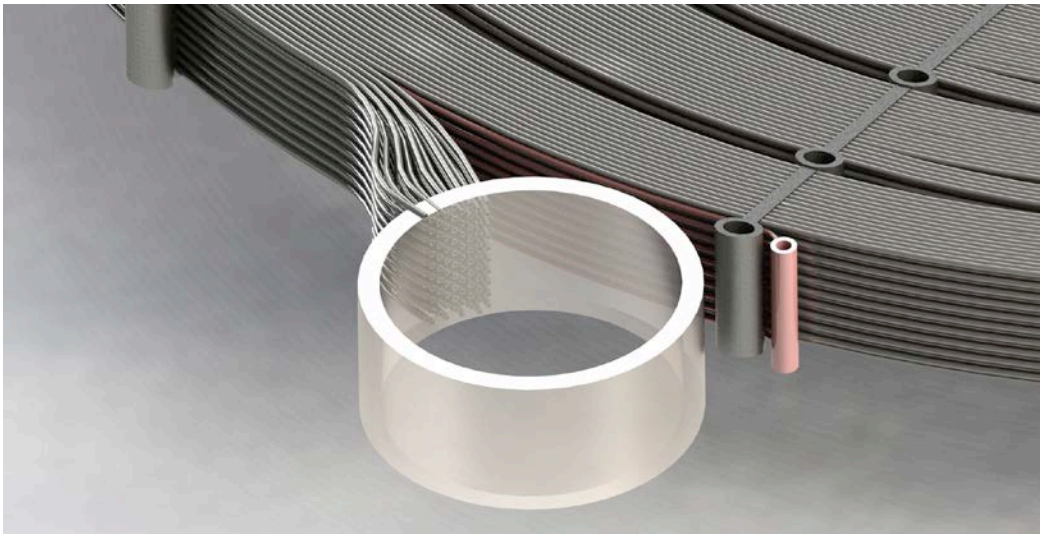

Figure 2. Close up view of tube to tube-sheet joints in a Mk1 CTAHs manifold pipe. Red cylinders are heater elements to control freezing under shutdown conditions.

The Mk1 CTAHs design proposed a novel method to fabricate the tube to tube-sheet joint, shown in Figure 3, where the end of the tube would be machined with a gentle taper, and inserted into a tube-sheet hole reamed to have the same taper angle. Our experiments show that insertion to a controlled depth can provide a strong friction fit, simplifying the bundle assembly, as well as applying the pressure necessary for diffusion bonding to occur. In experiments performed here, the taper on the tube was machined using a lathe, but automated tooling similar to a pencil sharpener would be used for actual commercial-use heat exchanger fabrication. While a seal weld at the end of the tube will create a leak-tight joint, the strength of the joint comes from high-temperature heat treatment of the bundle, to form diffusion bonding between the tube and tube-sheet. A key goal of this project was to demonstrate experimentally the creation of this type of diffusion bond.

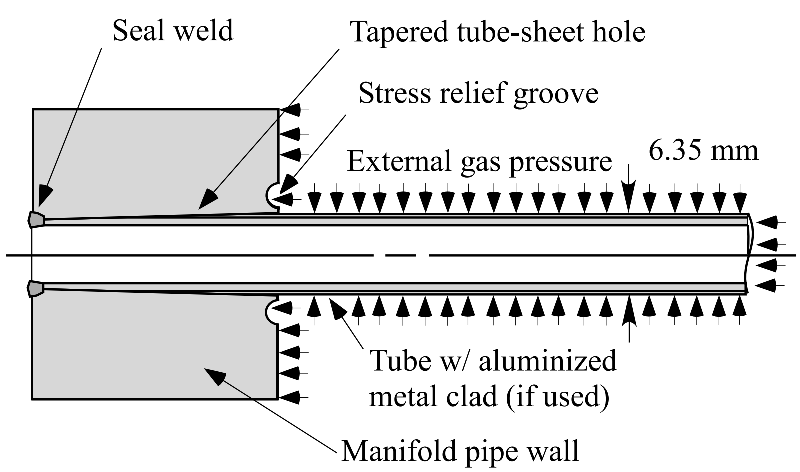

Figure 3. Schematic of a diffusion-bonded, seal-welded CTAHs tube to tube-sheet joint.

Because the pressure difference between the air and the salt in the Mk1 high-pressure and low-pressure CTAHs (5 to 18 atm) is relatively small compared to the typical pressure difference in steam generators (70 to 220 atm), the tubes can be designed to operate at a small fraction of the stress allowed under the ASME Boiler and Pressure Vessel Code (BPVC), as shown in Table 1. In addition, the CTAHs are relatively novel in that the tubes and the tube-sheets operate under compressive stress, whereas conventional steam generator tubes operate in tension. (The NuScale steam generators are uncommon, because they operate similarly – in compression.)

Table 1. Design stresses for Mk1 reactor vessel and CTAHs tubes, with a comparison to S-PRISM sodium fast reactor vessel (C. Andreades et al., 2014, Table 1-2).

	Reactor vessel	**HP CTAH tubes**	**LP CTAH tubes**	**S-PRISM reactor vessel†**
Outside diameter (cm)	350.0	0.635	0.635	919.5
Wall thickness (cm)	6.0	0.0889	0.0889	5.0
Maximum pressure differential (bar)	2.50	16.72	2.95	1.41
Circumferential stress (MPa)	7.30	5.97	1.05	13.01
Axial stress (MPa)	3.71	3.47	0.61	6.54
Von Mises stress (MPa)	6.32	5.19	0.91	11.26
Von Mises stress (ksi)	0.92	0.75	0.13	1.63
Nominal operating temperature (°C)	600	700	700	355
ASME allowable stress for 316 SS for 100,000 hr (MPa)	60.0	23.00	23.00	110.00
Ratio of allowable to actual stress	9.49	4.43	25.19	9.77

† Pressure differential for S-PRISM based upon sodium hydrostatic head of 16.7 m

While the CTAHs tubes operate with relatively low stresses, stress concentration occurs at the tube to tube-sheet joints. Optimizing the design of these joints to reduce stress concentrations is necessary. The pressure differential in the CTAHs creates a force to push the tubes into the tube-sheets, rather than loading them in tension as occurs in conventional steam generators. The use of tapered tubes and tapered tube-sheet holes is advantageous for this reason because they load the tapered joint in compression. Diffusion bonding can be effective in transferring shear stresses from the tube to the tube-sheet through these tapered joints. Diffusion bonding of metals has been studied extensively for other applications (Clark, D.E. and Mizia, R.E., May 2012). The effects of creep on un-bonded 316 SS have also been investigated (Harries, D.G. and Morris, D.R., 1978). One method to reduce the stress concentration where the tube enters the tube-sheet is to machine a stress relief groove into the tube around the tube, as shown in Figure 3. For the initial proof-of-concept experiment performed here, no groove was used, but future studies should examine joints fabricated to include these grooves.

CTAHs experience high operating temperatures and pressure differentials between the air and the salt. Therefore the CTAHs tubes and their joints will undergo time-dependent thermal and stress behavior over their life-cycle. Because thermal creep will occur, the capability to perform in-service inspection to monitor this degradation is critical. While the CTAHs tube bundles are designed to be replaceable, it is preferred that the bundles operate for the full life of the plant. Therefore predicting creep phenomena is also important. COMSOL was used in an attempt to simulate creep behavior (see Section 3.0) since it was impossible to perform creep testing in the time-frame of our design project.

In nuclear heat exchangers, it is crucial that the tubes be inspected periodically to detect potential degradation. Because CTAHs tubes are loaded in compression, they cannot rupture, but they still can experience potential corrosion, creep, and buckling. For nuclear steam generators, in-service inspection of the ~1.9-cm outside diameter (OD) tubes is performed using eddy current probes. In the Mk1 CTAHs systems, the tubes have a 0.64-cm OD with a radius of curvature associated with the bundle geometry. This project also demonstrates that a catheter-like probe can be inserted and maneuvered over distances of at least 6.7 m into CTAHs tubes, to enable in-service inspection (see Section 4.0).

2.0 DIFFUSION BONDING EXPERIMENT

One of the primary goals of this project was to experimentally demonstrate the possibility of creating a diffusion-bonded joint that would bond a tapered tube to a tube-sheet using 316 SS (see Figure 3). This section describes the processes we used to create diffusion bonds, the results, as well as recommended future work.

2.1 Prototype Manufacturing

The specific manufacturing processes that lead to the diffusion bond of a tapered tube and tube-sheet dictate the quality of the bond, and are therefore important. The four processes that lead to the diffusion bonded joints in the CTAHs bundles are the machining and finishing of the tapered tube, the tapered hole in the tube-sheet, the application of pressure between the two, and finally the heating process. In this section, we describe these processes in detail for our proof-of-concept prototypes.

Simplified 316 SS prototypes joints were fabricated to be representative of the Mk1 CTAHs tube to tube-sheet joint design. The baseline CTAH coiled tube is a 6.4-cm diameter tube with a 2 cm long, 1.0º taper at the end (see Figure 4). The tube-sheet was simulated using a 2 cm diameter, 2 cm thick cylinder with a 1.0º tapered hole drilled through it to match the tapered tube. These two parts were small enough to be machined and heated in small furnaces, yet still retained the proper Mk1 CTAHs design characteristics in order to generate valid results. Several tubes and tube-sheet samples were fabricated, but only two were machined accurately enough to be used in diffusion bonding experiments. They are assigned the designations TTS-1 and TTS-2 (Table 2) for the purpose of this paper.

Table 2: Diffusion Bonding Samples.

Sample Designation	Heating Medium	Time Heated (minutes)	Heating Temperature (°C)	Method of Finishing	dx (mm) (see section 2.3)
TTS-1	Air	1000	1000	Lathe Tool	1.0
TTS-2	Vacuum	1000	1000	Scotch-Brite*	1.1

*Note: Reference: (Scotch-Brite, 2014).

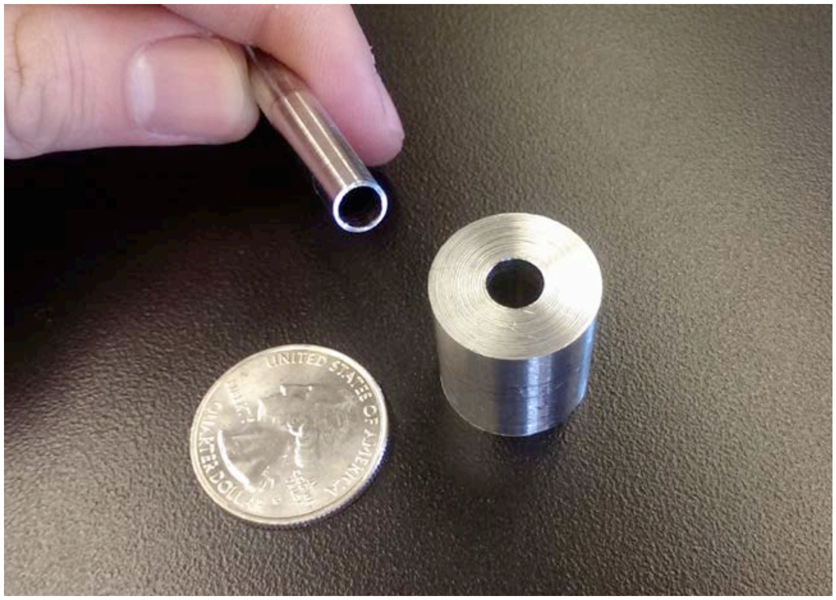
Figure 4. Prototype of the tapered tube and tube-sheet disk.

The tube was machined from 6.35 mm (1/4”) OD 316 SS cold-finished rod using a lathe. First, the lathe was adjusted so that the tooling feed operated at a 1° angle with respect to the rod. Next, a roughing tool was used to cut the taper to a few hundredths of a millimeter within the specified dimensions. A finishing tool was then used to turn the taper to specification. It was absolutely crucial for the feed rate to be as slow and steady as possible while machining the taper. A slower and more consistent feed rate yields a smoother surface finish, which results in a more uniformly parallel interface between the tube and tube-sheet. A 4.57-mm diameter, number 15 drill bit was used to drill the center hole with an inner diameter accurate to the design specifications. It would also be possible to use 316 SS tube directly.

It proved effective to use the same lathe, without changing the angle configuration of the feed in order to maintain identical parallel tapered surfaces between the prototype tube and tube-sheet disk. The tapered hole in the tube-sheet disk was made by center drilling, then drilling first with a number 15 bit, then a number 4 bit. The hole was tapered by using a small boring-bar. As with the tapered tube, the speed and consistency of the feed rate were critical to the surface finish.

Both the tapered tube-sheet hole and tube were surface finished using only the lathe cutting tools for TTS-1. For TTS-2, a Scotch-Brite Heavy Duty Scour Pad (Scotch-Brite, 2014) was used to polish the tapered surfaces, and remove any foreign material. All samples were cleaned using acetone before being press fit.

In order to join the tube to the tube-sheet with sufficient pressure to create a diffusion bond, the tube was press fit into the tube-sheet. Inadvertently the tapered hole was machined to have the same entrance diameter as the diameter of the tube, and thus the tube had to be over-inserted to achieve the correct compressive stress. For more information on this process, see Section 2.3.

The final process is to heat the two-part-assembly in a furnace. Two furnaces were tested, one that heated a partially polished sample in air, and another that heated a fully polished sample in a vacuum. Both furnaces were operated at 1000ºC for approximately 1000 minutes.

2.2 Proposed Fabrication Process For Commercial CTAHs

While the hand-machined prototypes had promising results, a precision-automated manufacturing process using custom tooling for the Mk1 CTAHs bundles would result in significantly stronger diffusion bonds, as well as a dramatically shorter manufacturing time.

The largest source of error in the prototype manufacturing processes was that of human machine operation. Manually machining parts on the lathe was effective for prototyping because it allowed freedom for design modifications as needed. However, the need for consistency among commercially-used parts creates the need for automation and custom tools. Figure 5 and Figure 6 illustrate two basic tool designs that could be used to create tapered geometries.

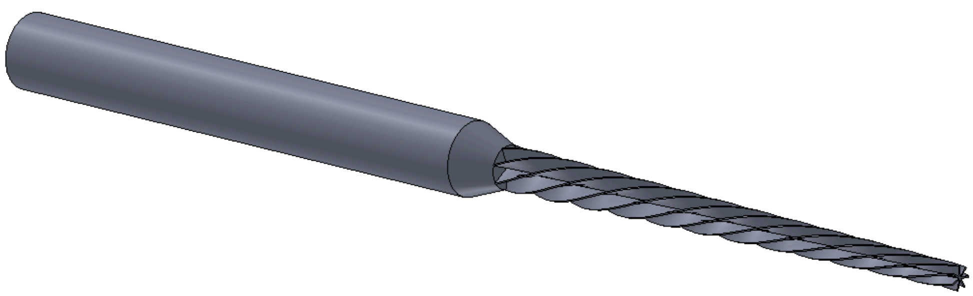

Figure 5. A seven-flute, 1º tapered reaming tool.

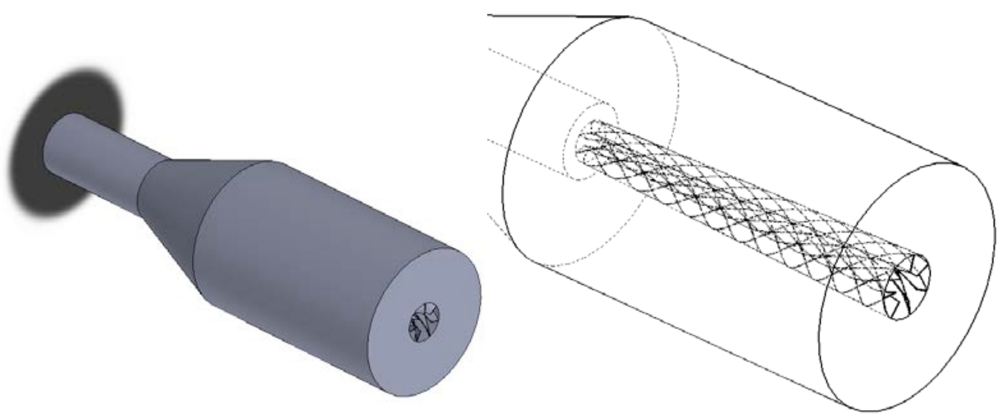

Figure 6. A seven-flute custom tool for machining 1º tapers onto 6.35mm tubes.

A Computer Numerically Controlled (CNC) machine performing a point-to-point operation could use the tool seen in Figure 5 to rapidly ream out multiple tapered holes into a tube-sheet. A tool similar to that in Fig. 6, or alternatively a tool similar to a pencil sharpener (see Figure 7) could used to machine tapers onto the tube ends. Both tools are designed with seven-flutes to ensure ease of steel machining as well as a smooth finish. Polishing tools of similar geometry could then be used to improve the surface finish on the tapers. The tubes would then be press fit into the tube-sheets, and the whole bundle would be heated in a large vacuum furnace.

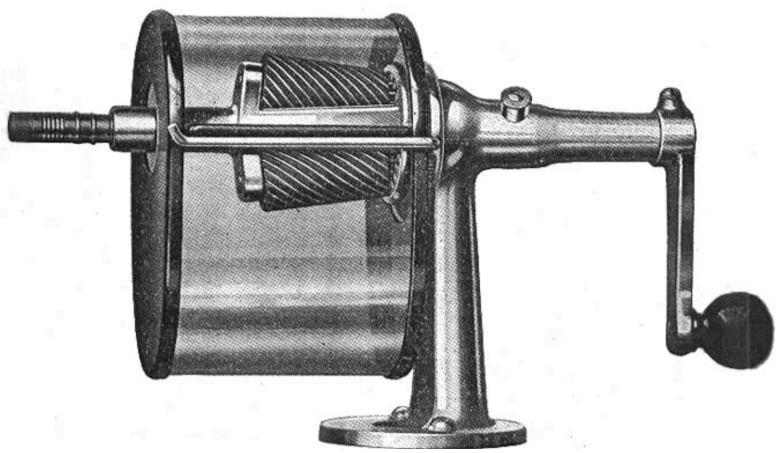

Figure 7. The internal mechanics in an old-fashioned pencil sharpener (Early Office Museum, 2014).

2.3 Pressure Application Method For Diffusion Bonding

The diffusion bonding process requires processing at high temperature while maintaining adequate contact pressure between the surfaces. Since it proves unwieldy to constantly apply a compressive load to a part in a furnace, it was proposed that a press fit of a tapered tube be used to apply the required pressure (Figure 8). This section analyzes the contact forces that can be generated using this method.

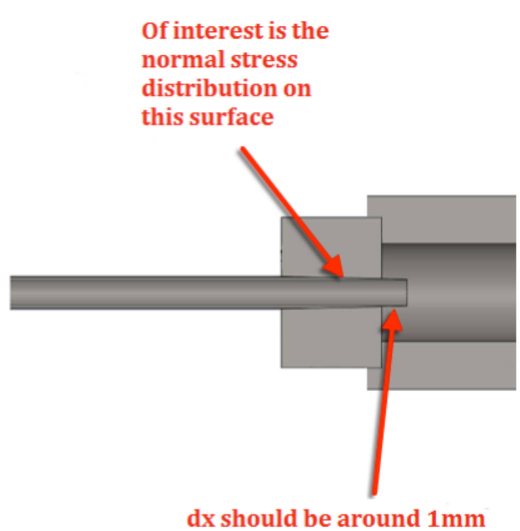

Figure 8. Press fit pressure analysis of the tube-to-tube-sheet joint. Note that dx is exaggerated in the figure. The actual fabrication design might be such that the tube ends up flush with the exit of the hole to simplify assembly control by obviating need for measuring the extruding portion of the tube.

Equation 1 (Slocum, 1995) was derived for an interference fit assembly, relating the contact pressure to unstressed diameters at any location of interest.

$$P = \frac{\left(D_{to} + \Delta_{t,+tol}\right) - \left(D_{si} - \Delta_{s,-tol}\right)}{\frac{D_{si}}{E_s}\left(\frac{D_{so}^2 + D_{si}^2}{D_{so}^2 - D_{si}^2} + \nu_s\right) + \frac{D_{to}}{E_t}\left(\frac{D_{to}^2 + D_{ti}^2}{D_{to}^2 - D_{ti}^2} - \nu_t\right)} \tag{1}$$

Where:

P	Interference pressure as a result of diametrical interference
D_{to}	Tube outer diameter
$\Delta_{t,+tol}$	Upper tolerance in the tube outer diameter
D_{ti}	Tube inner diameter
D_{so}	Diameter of tube-sheet disk
D_{si}	Diameter of hole in tube-sheet disk
$\Delta_{s,tol}$	Lower tolerance in the hole diameter
E_t	Young's modulus of tube material
E_s	Young's modulus of tube-sheet disk material
ν_t	Poisson's ratio of the tube material
ν_s	Poisson's ratio of the tube-sheet disk material

A stress distribution calculation with a thick-walled outer cylinder and a press fit inner tapered tube was done in MATLAB in order to characterize the depth (dx) to which the tapered tube should be pressed into the tapered hole on the tube-sheet disk to achieve a specified contact pressure. The geometry of the set-up and equation of interest are given in Figure 8**.** When the tube is pressed into the hole past the point of initial contact, the tube is loaded with a compressive stress. With 1.0º tapers on the tube and the hole in the tube-sheet disk over a length of 20 mm, this calculation shows that inserting the tube 1 mm into the hole in the tube-sheet disk, past the point of initial contact, will create a stress distribution on the contact surface as shown in Figure **9**. The amount of interference between the outer surface of the tube and the surface of the hole in the tube-sheet disk is shown in Figure **10**. Averaging this stress distribution over the contact area gives a value of 182 MPa, with a maximum stress of 257 MPa occurring close to the large-diameter side of the tapered hole. These values are below the 316 SS yield strength of 290 MPa. This result suggests that a 1 mm distance is a reasonable depth by which the tube could be pressed into the tube-sheet disk in order to generate the contact pressure required for successful diffusion bonding.

In our experiment, tapered tubes were pressed into tube-sheet holes manually with a bench vise. The initial point of contact was established by having the tapered tube slide freely into the tapered hole until it was completely blocked by the tube-sheet material. Even though the taper angle was kept constant for both parts, the smaller diameter of the tapered tube was machined to be smaller than that of the tapered hole, causing the tube to extend from the exit of the hole by a finite amount at the initial point of contact. This initial extension length was directly measured with a caliper. After the tube was manually pressed into the hole with the bench vise, the penetration depth dx was determined by subtracting the initial extension length from the new one.

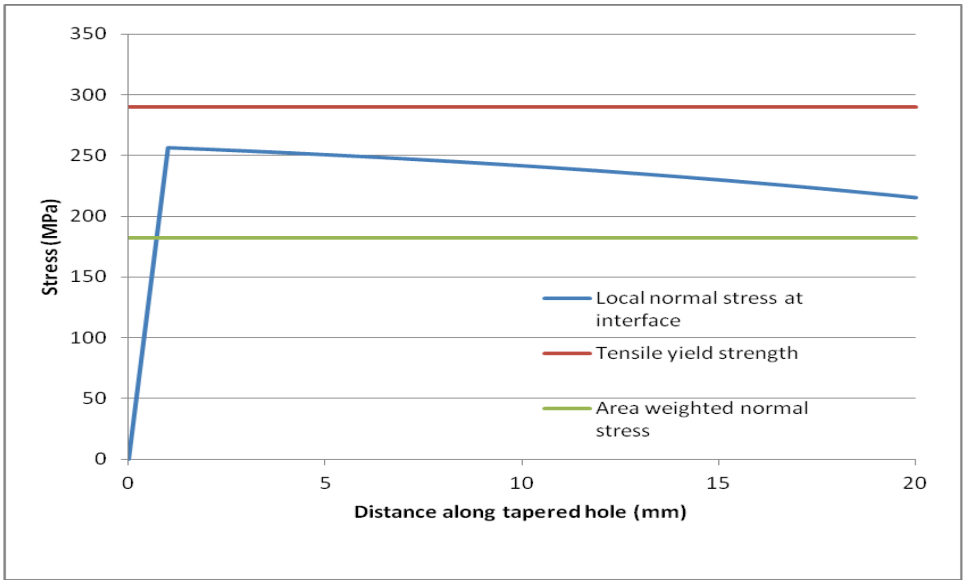

Figure 9. Press fit stress distributions with dx = 1 mm.

Figure **9** shows that the normal stress is zero at the entrance. This is caused by the fact that the larger diameter of the hole in tube-sheet disk was machined to be equal to the outer diameter of the tube. The resulting interference-free condition at the entrance creates a stress distribution in an entry region that starts from no stress at the entrance to a maximum value at the penetration depth dx. The low stress condition at the front end of this region is very likely the main cause of delamination effects observed after the tensile pull tests.

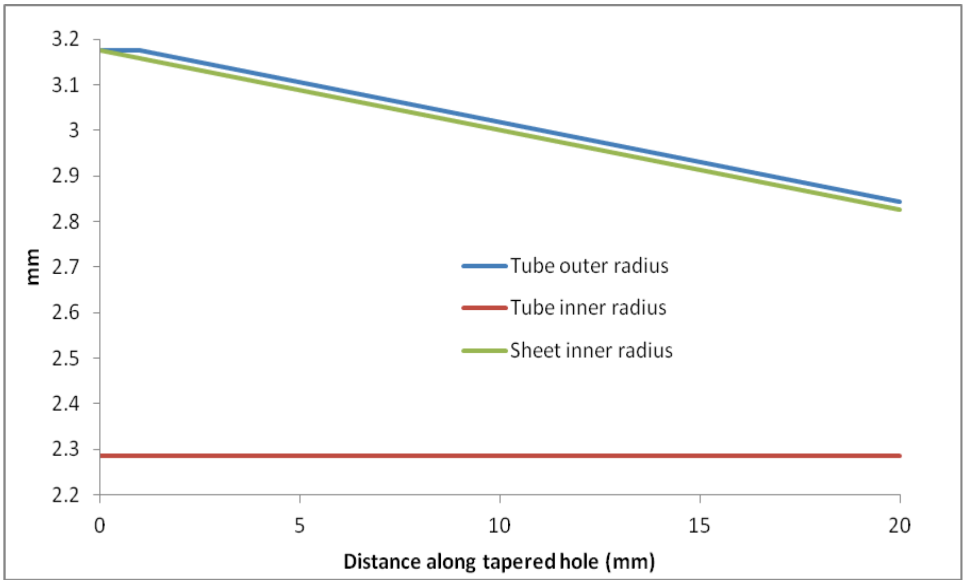

Figure 10. Press fit relative geometry with dx = 1 mm.

Figure **10** shows the relative positions of the tube and the hole in the tube-sheet disk under the notional assumption that they do not "see" each other. The interference-free condition at the entrance may be readily noticed.

2.4 Tensile Testing Setup

Important characteristics of the prototype diffusion-bonded joints were investigated by subjecting the samples to tensile pull tests until either the diffusion bond or the tube failed. Before the diffusion bonded joint was tested, the joint was assembled and subjected to tensile testing to measure the friction forces for the unbounded joint. A custom holder (Figure 11, middle) was machined from steel in order to accommodate the test samples in the testing machine. An MTS Criterion Model 43 tensile testing machine was used.

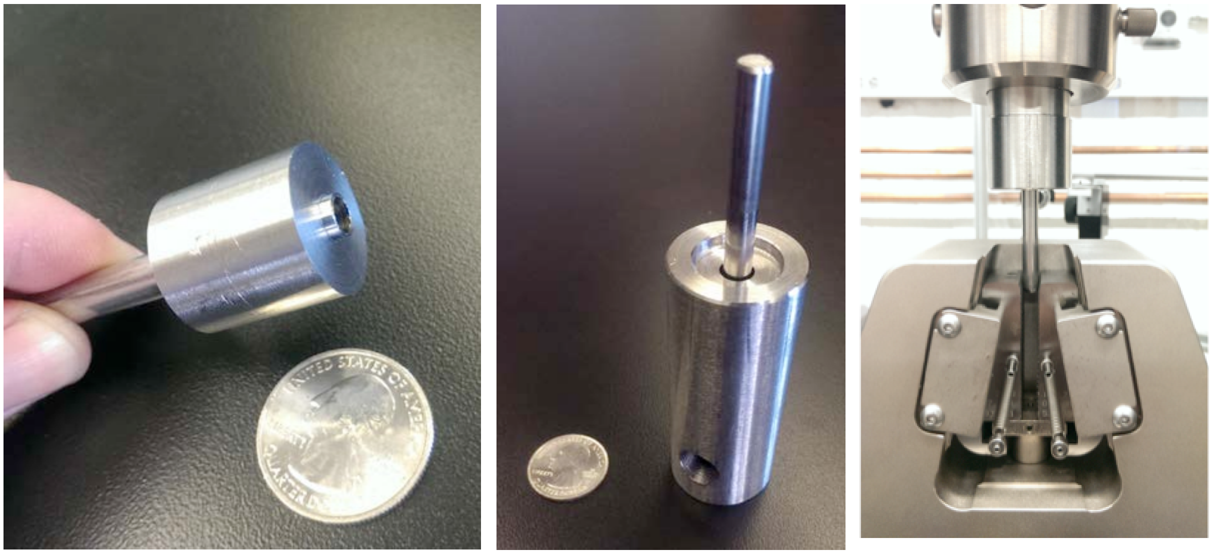

Figure 11. **Assembled sample (left), custom holder (middle), tensile strength testing apparatus (right).**

2.5 Quantitative Diffusion Bond Results

Results from TTS-1 and TTS-2 from Table 2 can be seen in Figure 12 and Figure 13. The "Pre-Heat" plots tested the strength of the press fit samples before heating, while the "Post-Heat" plots tested the strength of the diffusion bonded samples.

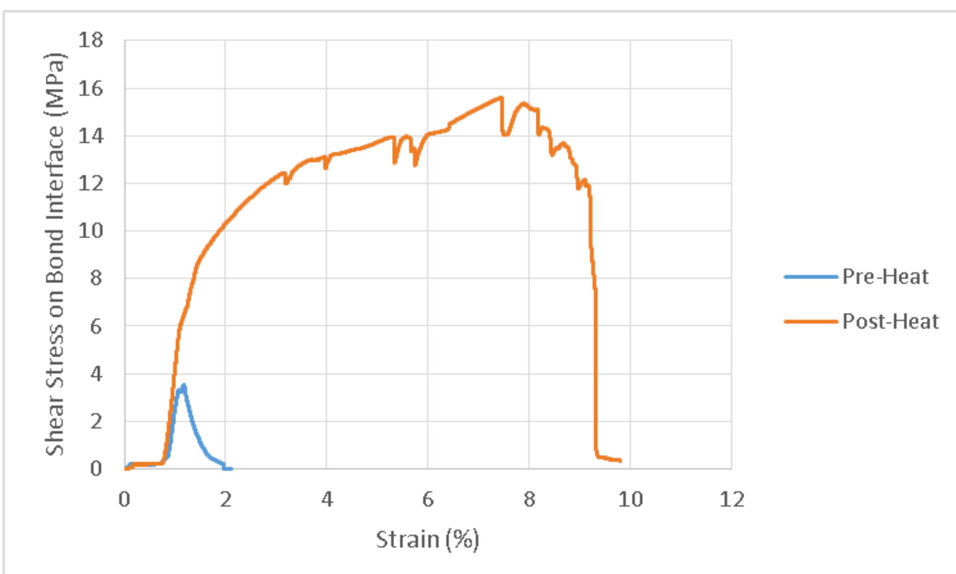

Figure 12. Tensile test results for TTS-1 heated in air at 1000ºC for 1000 minutes.

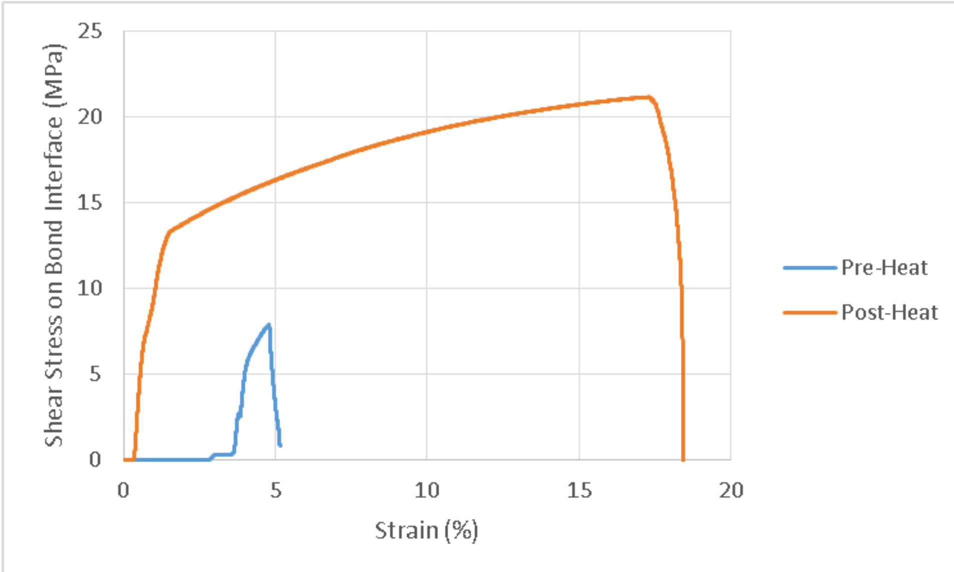

Figure 13. Tensile test results for TTS-2 heated in a vacuum at 1000ºC for 1000 minutes.

TTS-1 underwent a maximum tensile load of 6.23 kN before the bond interface yielded (see Figure 14), while TTS-2 underwent a maximum tensile load of 8.41 kN before the tube (not the bond) yielded. These maximum tensile loads for the air-heated and vacuum-heated samples are equivalent to 15.62 and 21.18 MPa, respectively.

2.6 Qualitative Diffusion Bond Results

Figure 12 contains interesting stress results for TTS-1. From approximately 3 to 9 percent strain, it appears that the TTS-1 bond underwent localized failures, resulting in decreased applied tensile load for small periods of time. The sample ultimately failed in the bonded region, as shown in Figure 14. Regions that appear to have been diffusion bonded can be seen in Figure 14. Some regions also appear to have resisted diffusion bonding due to imperfect polishing of the lathe-machined surfaces and the formation of oxidation layers. Figure 12 and Figure 14 both suggest that TTS-1 underwent localized diffusion bonding, but resisted a full diffusion bond due to the imperfect surface finish and the oxidation that occurred in the air furnace.

Figure 14: Diffusion bond failure in TTS-1.

TTS-2 provides us interesting results for several reasons. First and foremost, the sample failed in tension in the tube at the location where the tube was clamped, and not the diffusion-bonded interface. Because of this, the ultimate strength of the diffusion bond could not be measured. However, it was possible to section the sample axially and circumferentially, in order to characterize the bond interface qualitatively. The axially-sectioned sample is shown in in Figure 15.

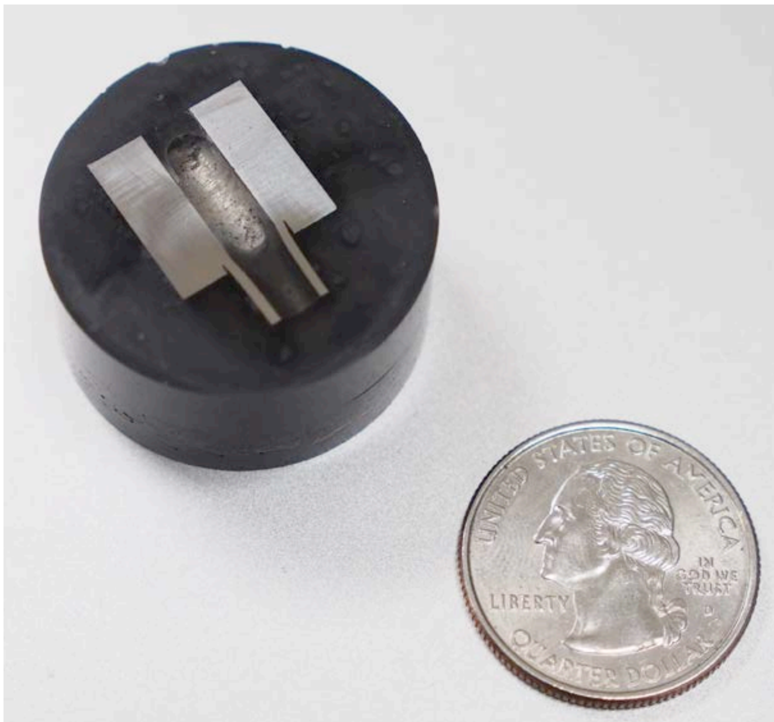

Figure 15 An axially-sectioned vacuum diffusion bonded sample TTS-2.

The sectioned sample seen in Figure 15 is invaluable because it shows the interface at which the diffusion bond occurred. The location at which the diffusion bond began to delaminate during tensile loading, as the tube necked down to a smaller diameter, can be seen. This delamination region is likely due to the stress distribution due to the press fit seen in Figure 9. The tapered hole was machined to have a large diameter equal to that of the tube. This resulted in zero applied stress during heating, which did not allow for a diffusion bond to form. In future tests, this delamination region could be eliminated.

While the delamination indicates that the diffusion bond was beginning to fail, it also indicates where the diffusion bond interface should be located. The sample was further polished using 1μm aluminum oxide polish, in order to examine the delamination region using optical microscopy. The result can be seen below in Figure 16.

10 μm

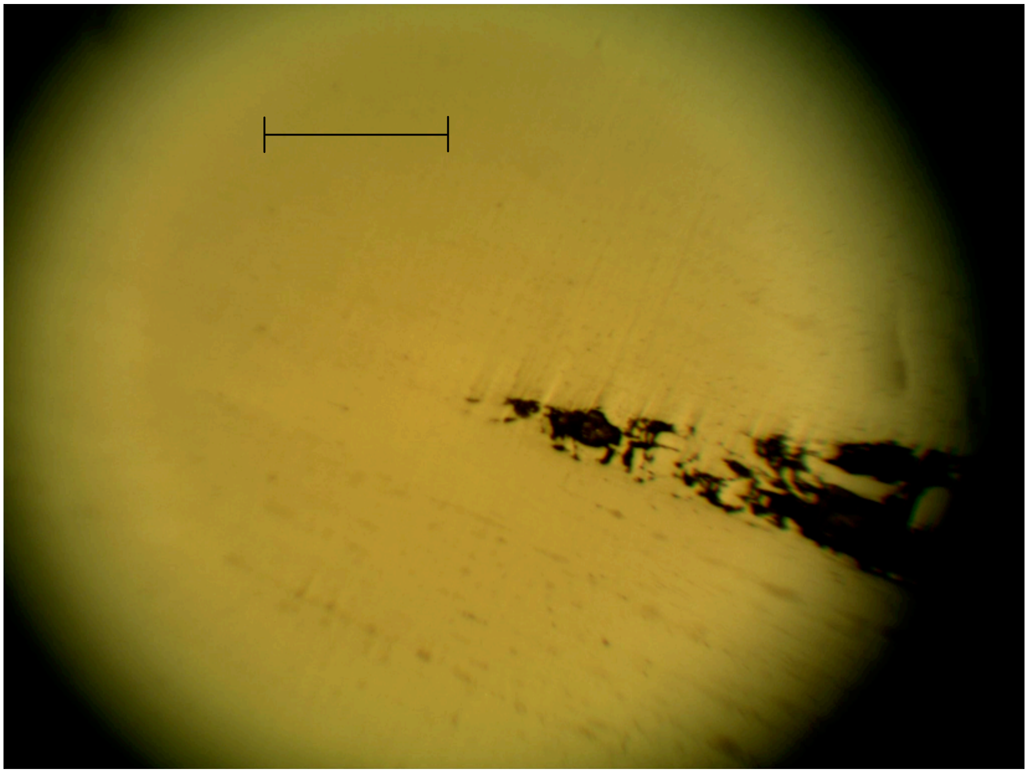

Figure 16. 20x optical microscope images of the delaminated region of the TTS-2 diffusion bond. Images show region in which diffusion bond interface should be able to be seen.

2.7 Discussion And Conclusions

The difference in maximum tensile loads seen in Figure 12 and Figure 13 between the pre-heated and post-heated samples clearly demonstrates the successful formation of diffusion bonds. The difference in maximum tensile load between the air-heated and vacuum-heated samples shows that a bond interface created in a vacuum with minimal contaminants generates a stronger bond.

During the press fit, the tube-sheet acted as a thick-walled cylinder, applying compressive stress on the tube. Figure 12 and Figure 13 show that this compressive stress was sufficient to create a diffusion bond. This result is particularly helpful for several reasons. First, no additional force was needed during the heating process to create a diffusion bond. Second, in the manufacturing of the Mk1 air heaters, the press fit will be strong enough to ensure that the tube bundle will stay joined to the tube-sheets until the entire CTAHs bundle is ready for heating. For a more detailed calculation of the stresses in the press fit, see Section 2.3.

These results support the hypothesis that the Mk1 CTAHs tube bundles can be manufactured using the diffusion bonding process. This experiment has shown that high-strength diffusion bonds can be created in the geometry unique to the CTAHs tube bundles. Further work will aim to ensure that these diffusion bonds will be able to withstand the long term heat and stress that the CTAHs bundles will undergo during reactor operation.

3.0 COMSOL FEM MODELING

Figure 17 and Figure 18 show COMSOL model of initial stationary (time-independent) von Mises stresses present in the prototype HP CTAHs joint as it is subjected to an external compressive pressure of 1.672 MPa (16.72 bar) (from Table 1) that is distributed along the joint as indicated in Figure 3. This model assumes a complete and ideal diffusion bond along the joint interface and simulates the tube and tube-sheet assembly as a single, homogenous body. The assumption is made according to the ideal final conditions of diffusion bonding; that is, two materials will become bonded into one homogenous material. Stress concentrations of approximately 12 MPa are highest along the axial length of the tube, suggesting the occurrence of creep strain that would decrease the tube radius. The stress relief groove shown in Figure 18 provides an effective stress relief for the high stress concentration illustrated in Figure 17 located at the surface edge of the tube-to-tube sheet interface.

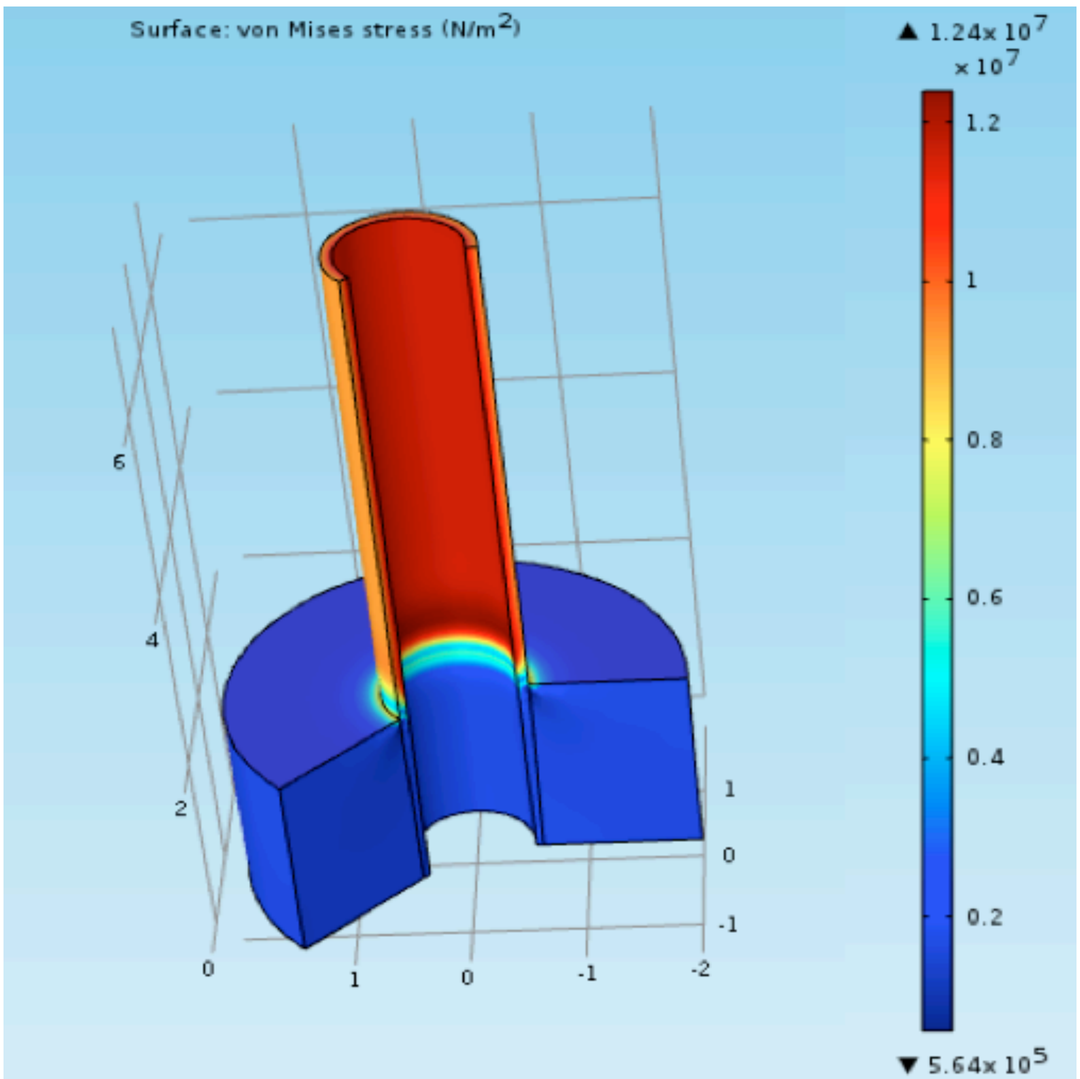

Figure 17. COMSOL model of von Mises stresses in CTAHs joint prototype (no stress relief groove).

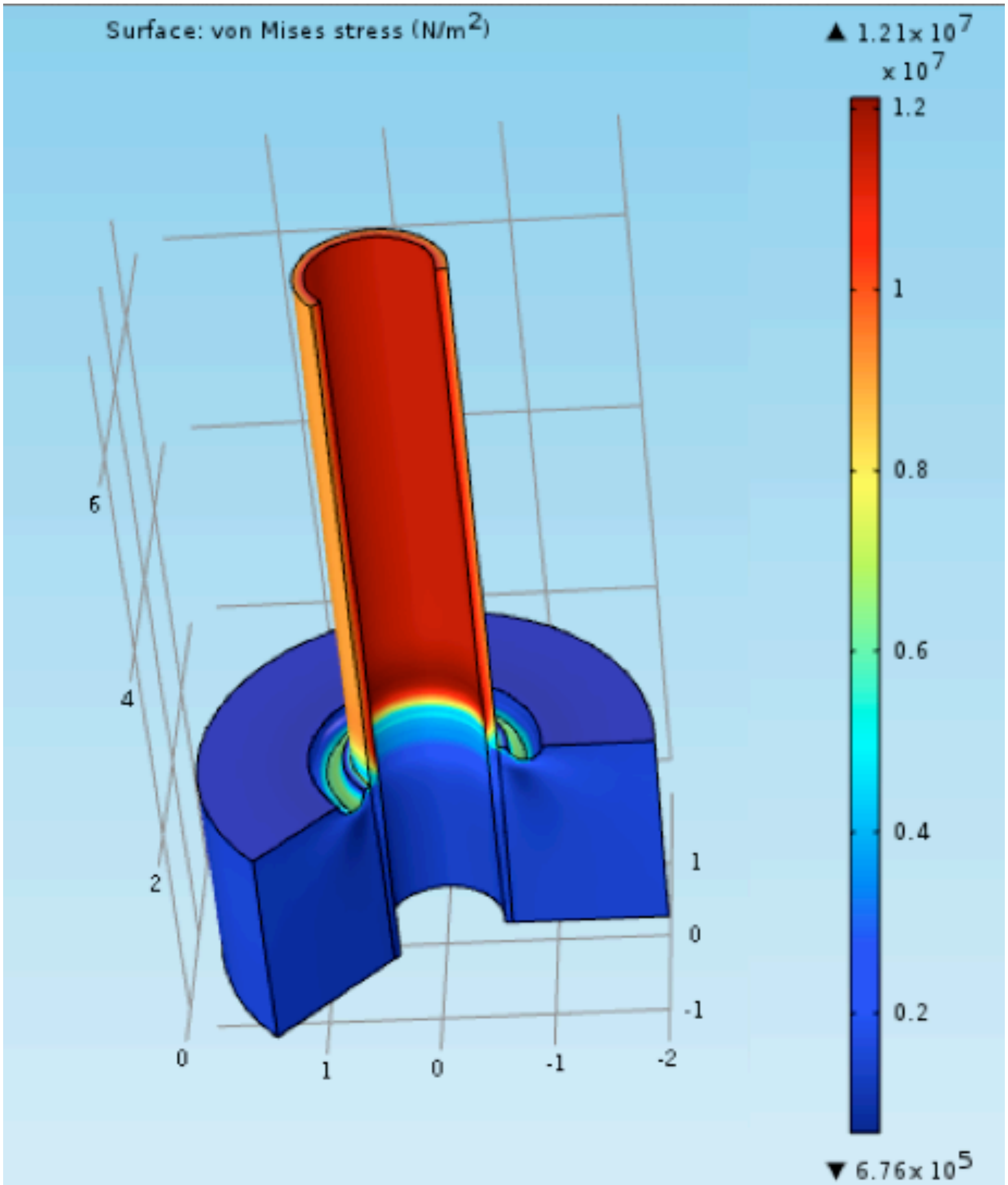

Figure 18. COMSOL model of von Mises stresses in CTAHs joint prototype (with stress relief groove).

4.0 MAINTENANCE TESTING

Since the inner diameter of the CTAHs tubes is only 4.57 mm, conventional commercial eddy current and remote field testing probes, as used in nuclear steam generators, are too large to be used for in-service inspection. In this experiment, we investigated the feasibility of tube inspection using eddy current probes. Two relevant methods, the selection of which is dictated by the tube material, are (Olympus NDT, 2010)

- Eddy current probe technology (Figure 19).
- Remote field testing (Figure 20).

In the eddy current probe method, an alternating current gets sent through in a coil in the probe and creates a time-varying magnetic field through electromagnetic induction. This magnetic field results in the formation of an eddy current in the wall, which in the presence of a defect, is distorted by a resulting change in impedance. A sensor located in the probe can pick up this distortion, signaling defect detection. The eddy current method only works for non-ferromagnetic materials such as copper, alloy N, aluminum, 316 SS, 304 SS.

In the remote field testing method, an exciter coil at one end of the probe sends out a magnetic flux which travels out of the tube wall, along the probe and then back through the wall to a receiver located at the other end. Loss of wall material due to a defect causes the back-travelling signal to reach it in a shorter time and have a greater amplitude. In contrast to eddy current testing, the remote field method only works with ferromagnetic materials such as 400 SS, carbon steel.

Both of these methods involve moving a cylindrical probe and probe cable through the tube under inspection. Standard eddy current probes such as those available from Olympus typically have an outer diameter exceeding the 4.57 mm inner diameter of the tube under inspection (Olympus NDT, 2012). An exception is probes designed for bolt-hole inspection that can have an outer diameter as small as 3.2 mm (Olympus NDT, 2010). This suggests that miniaturization of the probe itself is probably not as great a concern as that of other electrical components attached to it in the signal cable.

For a qualitative investigation, we deem it appropriate to simplify the problem to one that involves determining how far a cylindrical wire or tubing can be pushed into a coiled tube.

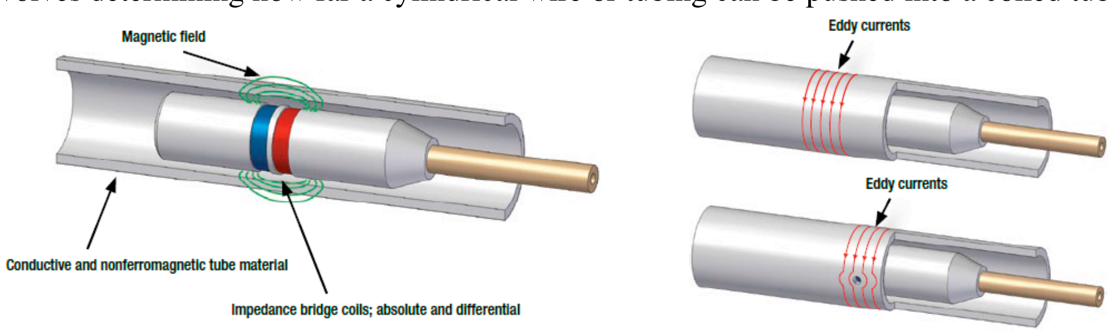

Figure 19. Eddy current testing.

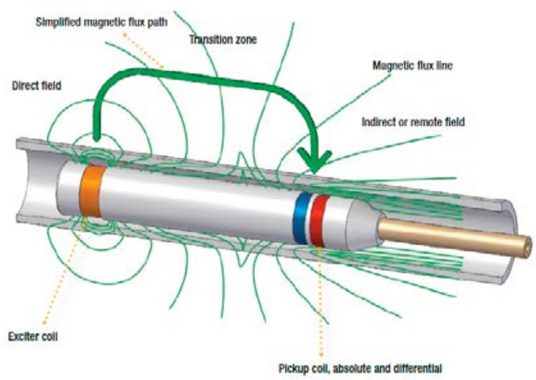

Figure 20. Remote field testing.

4.1 Experimental Setup

Two factors affecting the maximum insertion depth are the diameter of the probe cable and the coefficient of friction at the contact surface. The purpose of the experiment is to investigate the extent to which small wires and tubes (catheters) of different diameters and coefficients of friction can be inserted through a 7.62 m (25’) long 316 SS tube coil with a coiled diameter of 0.67 m. Data collected for aluminum, 302/304 SS, and galvanized steel wires and two Teflon® PTFE tubes are tabulated in Table 3. Teflon® Polytetrafluoroethylene (PTFE) tubes were selected due to its being the most ubiquitous fluoropolymer for medical vascular catheters. A very appealing characteristic of the material is that it has the lowest coefficient of friction of all catheter materials (Hartford, 2014).

These experiments were performed using a 4.57-mm ID, 316 stainless steel tube in a 0.67-m coil, with a length of 7.62 m. An experimental setup is shown in Figure 21. Qualitative results are expected to be similar to those obtained for longer (18 m) baseline CTAHs tubes since the baseline version has a larger coil diameter of about 2 m (hence reduced curvature).

Figure 21. An experimental setup consisting of a 0.67 m diameter coiled 316 SS tube that is 7.62 m long. Also shown is 3.18 mm outer diameter Teflon tubing partially inserted into the 316 SS tube.

4.2 Results

Table 3: Wire/tube insertion experiments on a 0.67-m diameter coil tube.

Material	**Type**	**Coefficient of Friction** (Handbook, 2006)	**Outer diameter (mm)**	**Length penetrated (m)**
Aluminum	Solid wire	0.61	1.6	1.5
302/304 SS Spring Back	Solid Wire	0.6 ± 0.18	1.3	1.9
302/304 SS Spring Back	Solid Wire	0.6 ± 0.18	2.0	0.61
Galvannealed steel	Solid Wire	0.6 ± 0.18	0.88	2.1
Teflon® PTFE	Tubing	0.04	1.5875	7.62
Teflon® PTFE	Tubing	0.04	3.175	7.62

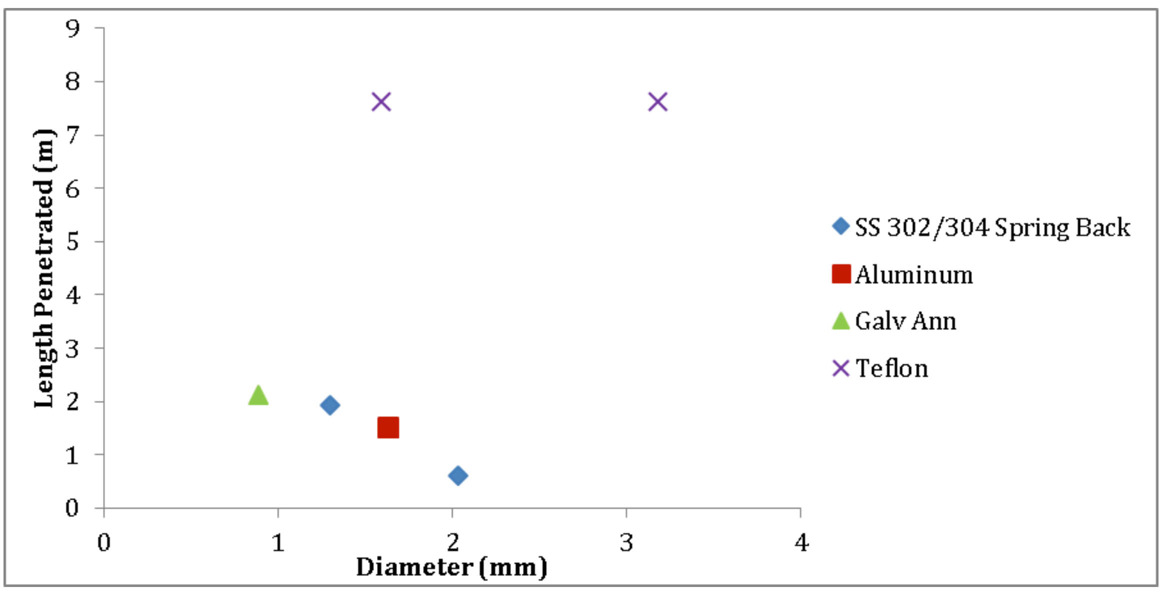

Figure 22. Plot of insertion depth vs. wire/tube diameter.

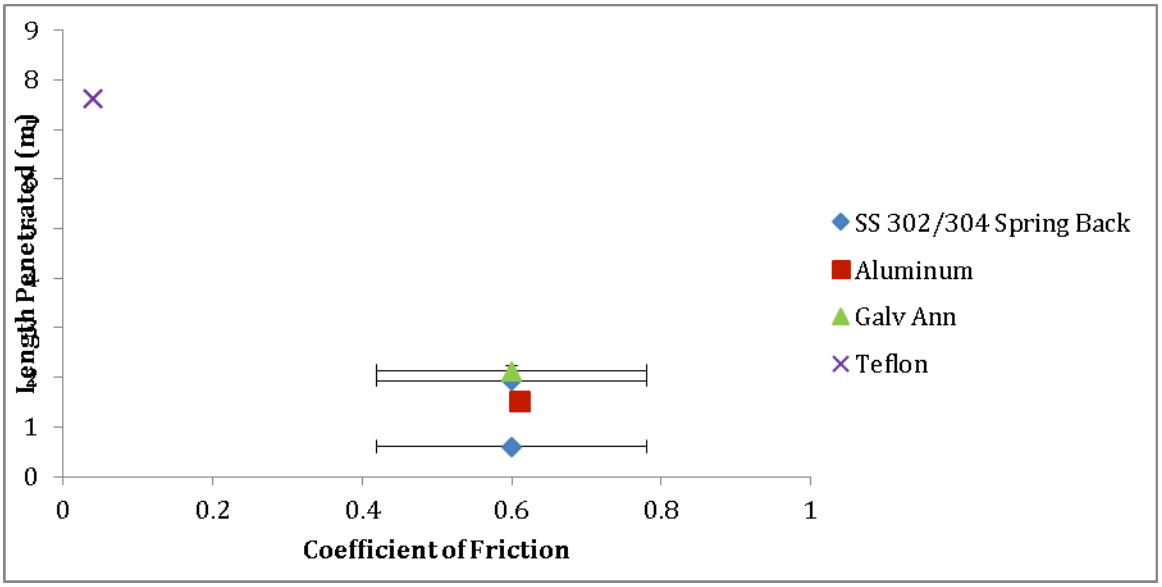

Figure 23. Plot of insertion depth vs. coefficient of friction on steel.

4.3 Discussion And Conclusions

For all non-Teflon data points presented in Figure 22, there seems to be a strong correlation between the depth of insertion and the diameter of the wires, namely, the depth of insertion decreases with increasing wire diameter. It should be noted that the coefficients of friction that correspond to these non-Teflon data points are very similar with mean values ranging approximately between 0.60 and 0.61. From the same figure, it can be seen that the Teflon® PTFE tubes present a clear exception to the aforementioned trend. This suggests the dependence of the insertion depth on diameter is at best important only for wires with similar coefficients of friction. Figure 23 shows that the coefficient of friction between the contact surfaces has a much stronger influence when limiting the maximum insertion depth.

From these results, we arrived at a conclusion that Teflon is a highly desirable material for tube inspection probe on account of its low coefficient of friction. During testing, however, we ran into a difficulty associated with removing the Teflon tubes after they had reached the maximum insertion depth. The Teflon tubes were eventually removed by giving them several sudden and forceful pulls. This problem may have unforeseen consequences and should be investigated further.

For future work regarding inspection of non-ferromagnetic tubes (316 SS or Alloy N), it is important to investigate and consider the feasibility of using eddy current Airgun probes such as those offered by Olympus NDT. These probes are designed to work with an Airgun probe pusher-puller, featuring a grooved design to reduce the pushing force in the tube end (Olympus NDT, 2014). They are intended to be used with an Airgun scanner to enable a fast inspection (4 m/s to 6 m/s push speed, and 2 m/s encoded pull speed). The core typically has a Kevlar braid to allow for hard pulls. The smallest custom-made probe diameter offered by this vendor is 11.4 mm, which is too large for our purposes. For this reason, miniaturization of this type of probe is a topic that requires further investigation.

5.0 RECOMMENDED FUTURE WORK

The ultimate goal of diffusion bonding is to subject two surfaces to such great heat and pressure that the grain boundaries migrate together and form a homogenous part, completely uniform with the rest of the material. Characterization of a diffusion bond requires evidence of grain boundary migration as a result of the bonding process.

Figure 16 shows no discernable seam between the two parts, which would appear to indicate a diffusion bond. This is however, not sufficient to characterize the bond completely. Further work must be done to expose and examine the grain boundaries of the two parts, in order to further characterize the bond. Acid etching or electro polishing are both recommended methods for further finishing the sectioned parts. A scanning electron microscope (SEM) should then be used to analyze the bond interface.

Future diffusion bonding tests would also include a stress relief groove (see Figure 3), and a tapered hole with smaller dimensions, in order to apply a large stress over the entire contact region (see Figure 9). These modification should eliminate the delamination region seen in Figure 15, and result in a full diffusion bond.

Creep behavior can be more accurately studied in COMSOL by taking into account the creep phenomenon's time and temperature dependence. The equation governing the rate of steady-state creep is given by Equation 2:

$$\ddot{\varepsilon} = A\sigma^{n}\exp(-Q/RT) \tag{2}$$

Where:

- $\ddot{\varepsilon}$ – creep strain rate
- Q – activation energy required to initiate creep
- A – material constant specific to 316 SS
- n – stress exponent specific to 316 SS
- T – temperature

By subjecting the CTAHs tube to tube-sheet joint CAD model to the expected Mk1 operating conditions (Table 1) and inputting known material parameters such as Q, A, and n directly into COMSOL's built-in creep program, the strain vs. time creep behavior can be accurately predicted.

Regarding maintenance testing for the CTAHs tubes, further work must be done to confirm that eddy current probe technology can be miniaturized to a sufficiently small package to be inserted into the coiled tubes. This will involve both a more detailed analysis of catheter insertion dynamics as well as the size-optimization of eddy current probe packaging.

6.0 SUMMARY

This project has created valuable data to support the manufacturing processes that are critical in the fabrication of the Mk-1 PB-FHR Coiled Tube Air Heaters. Specifically, it has been demonstrated experimentally that diffusion bonding is a viable attachment method for the tube to tube-sheet joints. This project has also determined significant parameters that affect the bond strength including surface finish of tapered parts, and the medium in which the diffusion bonds are formed. Prototypical manufacturing methods, as well as recommended methods for final production, have also been assessed. Sectioned diffusion bonded samples have been prepared for further analysis and will be helpful in ensuring strong diffusion bonds in the Mk1.

Preliminary FEM modeling of von Mises stresses indicate that the CTAHs joint can withstand the expected Mk1 operating conditions. Creep behavior is presumed to primarily occur in a manner that decreases the tube radius.

Additionally, this project has gathered initial data on the feasibility of different materials to be used as catheters when inspecting the CTAHs for maintenance. Specifically, Teflon has been highlighted as the coating material most likely to provide easy eddy current probe insertion.

7.0 REFERENCES

Andreades, C., Cisneros, A. T., Choi, J.K., Chong, A.Y.K., Krumwiede, D. L., Huddar, L.R., Huff, K., Laufer, M. R., Munk, M.O., Scarlat, R.O., Seifried, J., Zweibaum, N., Greenspan, E., and Peterson, P. F. (2014). *Technical Description of the 'Mark 1' Pebble-Bed Fluoride-Salt-Cooled High-Temperature Reactor (PB-FHR) Power Plant*. Department of Nuclear Engineering, U.C. Berkeley, Report UCBTH-14-002.

Clark, D.E. and Mizia, R.E. (May 2012). *Diffusion Welding of Alloys for Molten Salt Service – Status Report*. Idaho National Laboratory.

Early Office Museum. (2014). *Boston Pencil Pointer*. Retrieved from: http://www.officemuseum.com/sharpener_gallery_1910-1919.htm

Handbook, E. (2006). *Reference Tables -- Coefficient of Friction*. Retrieved from EngineersHandbook.com: http://www.engineershandbook.com/Tables/frictioncoefficients.htm

Harries, D.G. Morris and D.R. (1978). *Creep and rupture in Type 316 stainless steel at temperatures between 525 and 900°C Part I: Creep rate*. Metal Science, November, pp. 525-531.

Hartford, J. (2014). *New Extrusion Techniques Advance Catheter Design*. Retrieved from MDDI Medical Device and Diagnostic Industry: http://www.mddionline.com/article/new-extrusion-techniques-advance-catheter-design

Olympus NDT. (2010). *Advances In RFT Tube Testing Solutions*. Retrieved from Olympus: www.olympus-ims.com/data/File/rd-tech-probes/Advances_tube.en.pdf

Olympus NDT. (2010). *Eddy Current Probes and Accessories*. Retrieved from Olympus: http://www.olympus-ims.com/en/.downloads/download/?file=285213042&fl=en_US

Olympus NDT. (2014). *Eddy Current Airgun Probes*. Retrieved from Olympus: http://www.olympus-ims.com/en/tube-inspection-probes/ecairgun/

Scotch-Brite. (2014). *Heavy Duty Scour Pad*. Retrieved from Scotch-Brite: http://www.scotch-brite.com/wps/portal/3M/en_US/Scotch-BriteBrand/Scotch-Brite/Products/Product-Catalog/~/Heavy-Duty-Scour-Pad?N=4337+3294631680&rt=rud

Slocum, A. H. (1995). Precision Machine Design, © 1995. *Society of Manufacturing Engineers, Dearborn, MI*., 387-399.